Energy Conversion and Management: X 27 (2025) 101130

Contents lists available at ScienceDirect

Energy Conversion and Management: X

journal homepage: www.sciencedirect.com/journal/energy-conversion-and-management-x

"Kinetic modelling of biomass pyrolysis: A new lumped scheme for xylan-based hardwood hemicellulose"☆

Muhammad Yusuf Suleiman [a,1], Eleonora Benedetto [b,1], Veronica Piazza [b], Luca Lietti [b], Alessio Frassoldati [c], Tiziano Faravelli [c], Alessandra Beretta [b], Paulo Debiagi [a,*]

[a] Nottingham Ningbo China Beacons of Excellence Research and Innovation Institute, University of Nottingham Ningbo China, Ningbo 315100, PR China
[b] Laboratory of Catalysis and Catalytic Processes, Dipartimento di Energia, Politecnico di Milano, via La Masa 34, 20156 Milano, Italy
[c] CRECK Modeling group, Dipartimento di Chimica, Materiali e Ingegneria Chimica, Politecnico di Milano, Piazza Leonardo da Vinci 32, 20133 Milano, Italy

ARTICLE INFO

Keywords:
Xylan hemicellulose
Pyrolysis
Glucuronoxylan
Kinetic modeling
TGA
Biomass conversion
Bio-oil

ABSTRACT

Hemicellulose pyrolysis plays a critical role in biomass conversion processes, but its kinetic modeling remains challenging due to its structural complexity, variability across biomass sources and the lack of experimental speciation data. This study presents a new lumped kinetic model for the pyrolysis of xylan-based hardwood hemicellulose. The new model is developed using new experimental data obtained through a thermogravimetric analysis (TGA)-based methodology. The experimental setup allowed for high-precision measurement of devolatilization rates and quantitative product speciation under varying heating rates (3–100 °C/min). This enables the development of a new kinetic model stemming from a previously established lumped kinetic model for hemicellulose pyrolysis. The new model incorporates an improved feedstock characterization, modifies reaction pathways to better reflect experimental observations, and improves predictions of water, char, and bio-oil yields. Model validation was performed against independent literature data, demonstrating significantly improved accuracy over previous models, particularly in predicting gas evolution and bio-oil composition. The refined kinetic model enhances our understanding of hemicellulose pyrolysis mechanisms and provides a reliable tool for biomass conversion modeling, with implications for bioenergy and bio-based chemical production.

1. Introduction

Global conflicts and supply chain disruptions have highlighted vulnerabilities in conventional energy resources, urging the need for decentralized and renewable energy solutions [1]. Moreover, the transition to renewable resources like biomass will also reduce greenhouse gas emissions by substituting carbon-intensive fossil fuels. Biomass, particularly residual biomass, presents a promising renewable resource for energy and chemicals due to its abundance, sustainability, and carbon neutrality when managed properly. Residual biomass, such as agricultural waste, forestry residues, and by-products of food industry, can be valorized through thermochemical processes, including pyrolysis, combustion and gasification [2]. Among these processes, pyrolysis plays a fundamental role as it represents the primary step in all these processes and for this reason, it is a key focus of research in the field of biomass thermovalorization. Pyrolysis allows the utilization of biomass for heat and power generation, and for its conversion into biofuels and bio-based chemicals, providing alternatives to fossil fuels and petrochemicals, and contributing to a circular economy by reducing wastes [3]. Furthermore, it allows producing biochar, a valuable product for carbon sequestration and soil amendment [4].

Even though thermochemical processes are among the most effective methods for treating biomass feedstocks, these remain challenging to be processed due to their heterogeneous and complex structural and chemical nature. Biomass is typically composed of cellulose, hemicellulose, lignin, and various extractives, including lipids, proteins, phenolic compounds and sugars [5]. The proportions of these constituents vary significantly depending on the biomass source, greatly influencing its behavior during the pyrolysis process.

Hemicelluloses are a diverse group of polysaccharides with significant structural variability, as represented in Fig. 1: hardwood hemicellulose are mainly composed of glucuronoxylan, but also glucomannan

☆ This article is part of a special issue entitled: 'Biofuels' published in Energy Conversion and Management: X.

* Corresponding author.
E-mail address: Paulo.Debiagi@nottingham.edu.cn (P. Debiagi).

[1] Both equally contributed to this work.

https://doi.org/10.1016/j.ecmx.2025.101130
Received 31 March 2025; Received in revised form 28 May 2025; Accepted 30 June 2025
Available online 2 July 2025

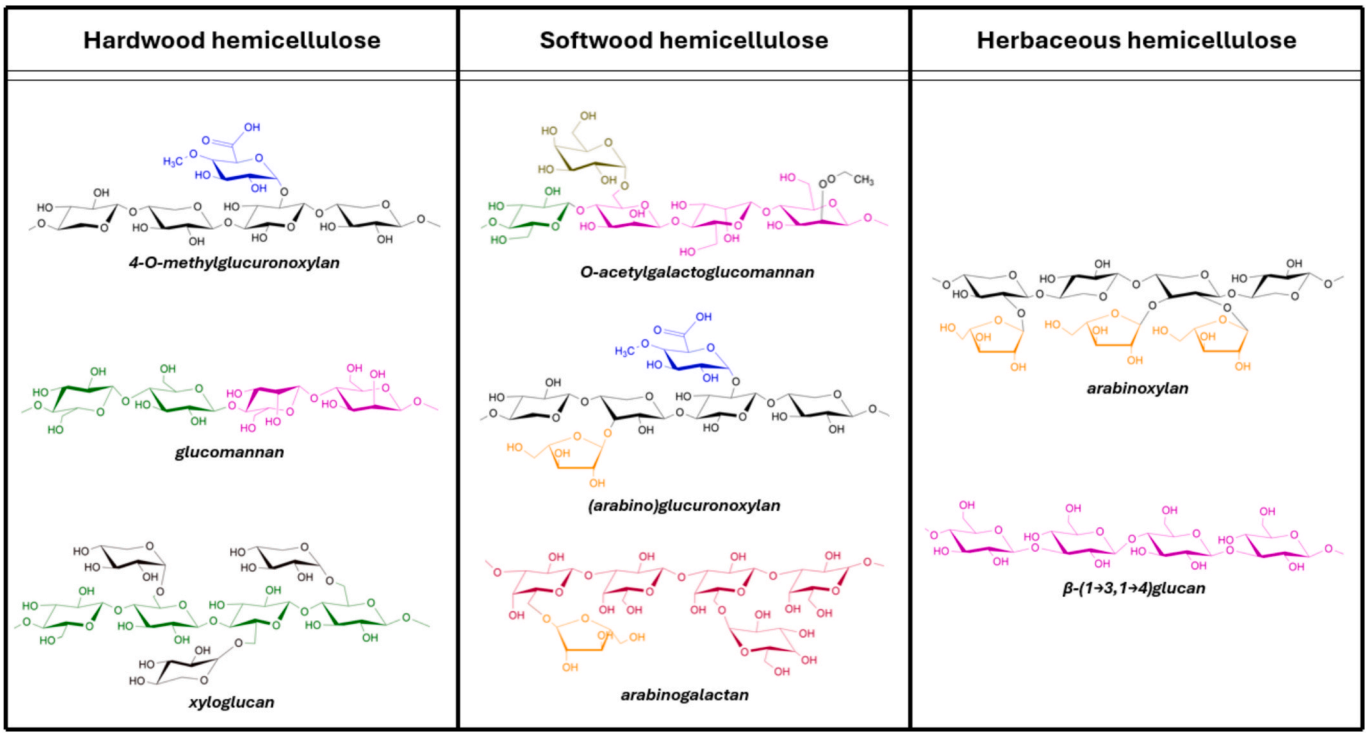

Fig. 1. Structure of common hemicellulose polysaccharides in hardwood, softwood and herbaceous biomass with corresponding monomers: black = xylose, blue = methyl-glucuronic acid, green = glucose, pink = mannose, orange = arabinose, red = galactose, brown = acetyl-galactose (figure []. (For interpretation of the references to colour in this figure legend, the reader is referred to the web version of this article.)
adapted from 6)

Table 1
Properties of xylan sample tested in this study.

Beechwood xylan (glucuronoxylan) properties	
Sugar composition	Xylose: 80.8 % Glucuronic acid: 11.4 % Other sugars: 7.8 %
Molecular structure	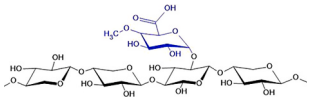
Elemental analysis	C: 39.97 ± 0.2 [wt%] H: 6.77 ± 0.2 [wt%] O: 53.26 [wt%] N: <0.01 [wt%]
Proximate analysis	Moisture: 11.5 [wt%] Volatile matter: 66.3 [wt%] Fixed carbon: 18.8 [wt%] Ashes: 2.6 % [wt%]

and xyloglucan are present. Glucomannan is instead the most abundant component in softwood hemicelluloses, together with smaller fractions of glucuronoxylan and arabinogalactan. Finally, arabinoxylan is the major hemicellulose in herbaceous hemicelluloses. Among them, xylan-type hemicelluloses represent the most abundant ones and they are for this reason often chosen as a reference component in literature studies [7–11]. Xylan –based hemicelluloses can be broadly classified according to the presence and distribution of substituent groups on the main xylosyl backbone. Glucuronoxylan features a single glucuronic acid substituent for every ten to fifteen xylose units [12], along with a variable number of acetyl groups. In contrast, xylan-based hemicellulose found in the primary cell walls of dicots follows a more regular pattern, with one glucuronic acid substitution for every six xylose units. Monocots exhibit a similar ratio of one glucuronic acid for every four to six xylose units [13]. Another major xylan-based hemicellulose is glucuronoarabinoxylan, commonly found in grasses and gymnosperms. It is characterized by an abundance of arabinofuranose side chains, with a smaller number of glucuronic acid substitutions [12].

During pyrolysis, xylan-based hemicelluloses undergo decomposition, resulting in the formation of a solid char residue (composed of fixed carbon and ash) and a variety of volatile products. These volatiles include both condensable and non-condensable species, ranging from small molecules such as CO, CO_2, short-chain alcohols, aldehydes, and carboxylic acids to larger organic compounds, including furan-ring derivatives and anhydrosugars [14]. The thermal degradation of xylan-based hemicelluloses is a complex process involving multiple simultaneous reactions, such as dehydration, depolymerization, fragmentation, and carbonization [15]. Various decomposition pathways have been proposed and summarized in studies by Shen et al.[7] and Zhou et al. [16].

Due to its commercial availability, beechwood extracted glucuronoxylan (commercially named "beechwood xylan") has been commonly used as a model compound for hemicellulose pyrolysis studies [7,10,17,18]. Thermogravimetric analyses (TGA) of beechwood xylan present in literature show a major weight loss in the range of 190–350 °C, depending on the heating rate. Differential scanning calorimetry (DSC) experiments have further revealed that its decomposition is associated with exothermic charrification reactions [19]. Product analysis from beechwood xylan pyrolysis has been performed using techniques such as Fourier transform infrared spectroscopy (FT-IR) and gas chromatography-mass spectrometry (GC–MS/FID) [7,20]. The gaseous phase is predominantly composed of CO, CO_2, and CH_4, while the bio-oil contains a complex mixture of carboxylic acids, furans, aldehydes, ketones, cyclopentanone and water. Some studies have also reported on the presence of anhydrosugars; however, conflicting results exist in literature regarding their formation [21].

Despite the importance of xylan as a representative hemicellulose polysaccharide and its significant presence in biomass feedstocks, literature data on its pyrolysis remain fragmented. This gap in

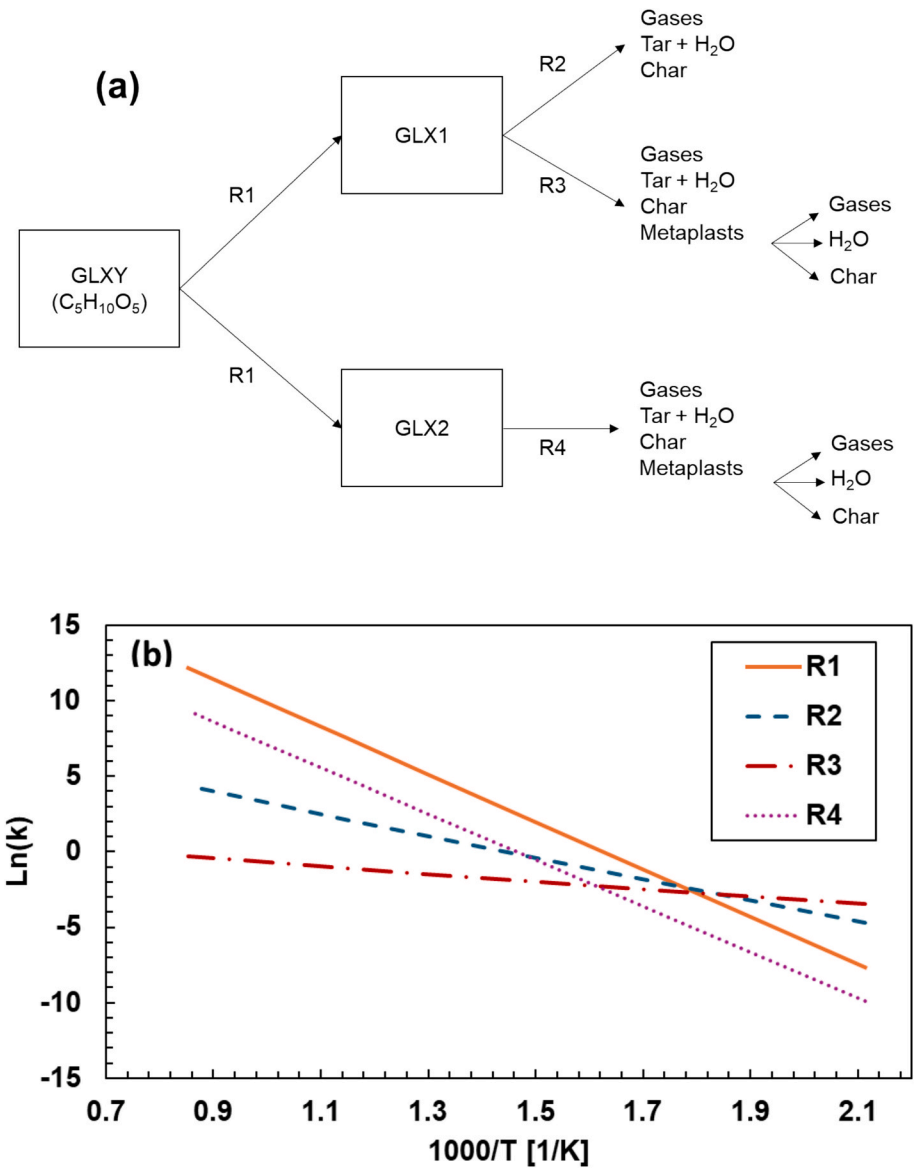

Fig. 2. (a) CRECK-S scheme for glucuronoxylan pyrolysis (b) Arrhenius plots of the rate constants reported in Table 2.

knowledge highlights the need for accurate, comprehensive, and quantitative data to advance our understanding of biomass pyrolysis and develop reliable kinetic models.

In fact, developing predictive kinetic models for biomass conversion processes is crucial for optimizing thermochemical technologies and for improving reactor design, process efficiency, and product yield control. In this respect, lumped kinetic models offer a good compromise between computational efficiency (facilitating integration with reactor simulations) and sufficient accuracy for engineering applications, especially when compared to mechanistic models based on elementary reaction pathways at the molecular scale. Lumped kinetic models of hemicellulose pyrolysis were initially proposed by some of the authors [22–24] and are now being refined thanks to the new experimental findings. The CRECK-S kinetic model initially proposed a representation of all hemicellulose types with a single component, defined as a polymeric chain of pentose monomers [24]. This simplification caused misprediction in the pyrolysis behavior of several feedstocks. The model was later improved, differentiating hemicelluloses that originate from hardwood, softwood and grass/cereal feedstocks [23,25], following the approach suggested by Dussan et al. [26].

In a recent study, some of the authors studied the pyrolysis of xylan using a novel TGA-based methodology, which allowed for the collection of a high-quality, quantitative dataset with strong kinetic relevance, in terms of both devolatilization rate and product speciation [18]. A preliminary comparison between experimental data and the state-of-the-art lumped models (Debiagi et al. [23] and Dussan et al. [26]) revealed that both models adequately predict the devolatilization trends of xylan pyrolysis, but they fail to describe the distribution of pyrolysis products, especially for tar species.

To address these gaps, the present work proposes a new lumped model for the pyrolysis of glucuronoxylan hemicellulose, addressing critical gaps in the prediction capability and reliability of the model, especially in terms of product speciation. The model was developed using accurate and complete datasets collected with the novel TGA-based experimental methodology [27], using a reference xylan compound with a well-defined molecular structure.

The paper is structured as follows: first, the Materials and Methods section details the experimental setup and the lumped kinetic model. The Results and Discussion section instead analyzes the response of the model, comparing it with newly collected experimental data and a previous version of the kinetic model for hardwood hemicellulose, highlighting improvements. The new model is also validated by

Table 2
Kinetic scheme of the new glucuronoxylan model.

	Kinetic Mechanism	Kinetic Parameters A [1/s], E_{act} [kcal/kmol]
R1	GLXY → 0.35 GLX1 + 0.65 GLX2	$1.25 \times 10^{11} \times$ Exp (−31400/RT)
R2	GLX1 → 0.05 $C_5H_8O_4$ + 0.16 FURFURAL + 0.18 CH_3COCH_3 + 0.09 CO_2 + 0.1 CH_4 + 2.79 H_2O + 0.66 CO + 0.05 CH_3CHO + 0.1 CH_3CO_2H + 0.15 $C_4H_6O_2$ + 0.06 CH_2OHCH_2CHO + 0.02 H_2 + 1.48 CHAR	$1.6 \times 10^{1} \times T \times$ Exp (−12900/RT)
R3	GLX1 → 1.84 H_2O + 0.7 CO_2 + 0.22 CO + 0.21 G{CO} + 0.21 G{CO_2} + 0.05 H_2S + 0.11 CH_2O + 0.43 CH_2OS + 0.1 CH_4 + 0.525 G{CH_4} + 0.1 C_2H_4 + 0.075 G{C_2H_4} + 1.375 CHAR + 0.37 G{COH_2} + 0.2 G{C_2H_6}	$3 \times 10^{-3} \times T \times$ Exp (−3600/RT)
R4	GLX2 → 0.1663 CO + 0.5398 CO_2 + 1.7571 H_2O + 0.0305 C_2H_5OH + 0.0423 CH_2OHCHO + 0.015 CH_3CO_2H + 0.0178 MEK + 0.0178 CH_2O + 0.0238 $C_5H_{10}O_2$ + 0.1213 $NC_5H_{10}O$ + 0.7 G{H2O} + 0.0912 G{CH_4} + 0.01 G{CO} + 0.0312 G{CH_3OH} + 0.0158 G{C_2H_4} + 0.20 G{CO_2} + 0.0337 G{CH_2O} + 2.345 CHAR + 0.7 G{H_2} + 0.3792 G{COH_2} + 0.0445 G{C_2H_6}	$5 \times 10^{9} \times$ Exp (−30500/RT)
R5	G{CO_2} → CO_2	$1 \times 10^{6} \times$ Exp (−24500/RT)
R6	G{CO} → CO	$5 \times 10^{12} \times$ Exp (−52500/RT)
R7	G{CH_3OH} → CH_3OH	$2 \times 10^{12} \times$ Exp (−50000/RT)
R8	G{CH_2O} → 0.8 CHAR + 0.8 H_2O + 0.2 CO + 0.2 H_2	$6 \times 10^{10} \times$ Exp (−50000/RT)
R9	G{C_2H_6} → C_2H_6	$1 \times 10^{11} \times$ Exp (−52000/RT)
R10	G{CH_4} → CH_4	$1 \times 10^{11} \times$ Exp (−53000/RT)
R11	G{C_2H_4) → C_2H_4	$1 \times 10^{11} \times$ Exp (−54000/RT)
R12	G{COH_2} → 0.2 CHAR + 0.2 H_2O + 0.4 CO + 0.8 H_2 + 0.4 CO_{STIFF}	$1 \times 10^{9} \times$ Exp (−59000/RT)
R13	G{CO}$_{STIFF}$ → 0.8 CO + 0.2 CHARO	$1.8 \times 10^{8} \times$ Exp (−65000/RT)
R14	G{H_2} → H_2	$1.8 \times 10^{8} \times$ Exp (−70000/RT)
R15	MOIST → H_2O	$1 \times 10^{1} \times T \times$ Exp (−8000/RT)
R16	G{H_2O} → H_2O	$1 \times 10^{6} \times$ Exp (−22500/RT)

comparing its predictions with independent datasets from the literature to further establish its reliability and applicability. Finally, mechanistic insights behind the product formation mechanisms were highlighted.

2. Materials and methods

2.1. Structural and chemical analysis of the xylan feedstock

Pyrolysis experiments were performed on high purity (95 %) beechwood-derived xylan purchased from Megazyme International.

Table 1 reports the properties of the xylan tested in this study. For what concerns the monosaccharide composition, the sample is characterized by a xylose to glucuronic acid ratio of 7.6, and a 7.8 wt% content of other sugar compounds, as reported in the technical datasheet provided by Megazyme. Therefore, this hemicellulose is glucuronoxylan. The proximate analysis was carried out in a thermogravimetric analyzer (Hitachi STA7300 TG-DTA) following the ASTM method D7582-12. The elemental analysis was performed using an Elemental Analyzer Costech ECS model 4010, which enabled the simultaneous determination of C, H, and N content, which turned out to be below the instrumental accuracy. The O content was calculated as the complementary fraction. Char samples were collected from multiple pyrolysis tests at 100 °C/min up to 950 °C, followed by a cooling to room temperature in N_2 flow.

2.2. TGA- based experimental setup for pyrolysis experiments

Pyrolysis experiments were carried out using a novel TGA-based methodology developed by Piazza et al. [27] to obtain kinetically relevant data on biomass pyrolysis. Initially developed and validated for cellulose, this methodology is here adopted for glucuronoxylan pyrolysis. The use of TGA in this setup ensures precise temperature control while eliminating heat and mass transfer limitations due to the small sample size. Additionally, the absence of secondary gas-phase reactions allows for the intrinsic measurement of devolatilization rates and product speciation. As a result, this approach provides quantitative and accurate data under various operating conditions, making it a powerful tool for the development and refinement of kinetic models.

Pyrolysis experiments were performed using a thermogravimetric analyzer (Hitachi STA7300 TG-DTA), where glucuronoxylan samples of 10–12 mg were placed inside a ceramic crucible and heated up at five different heating rates (3 °C/min, 10 °C/min, 20 °C/min, 50 °C/min, and 100 °C/min) with a helium (He) flow rate of 275 ml(NTP)/min, needed to suppress secondary reactions of the released products. Sample weight was continuously monitored, producing thermogravimetric (TG) and differential thermogravimetric (DTG) curves to evaluate devolatilization rates and determine the solid residual.

The liquid fraction of glucuronoxylan pyrolysis products (i.e., oxygenated compounds in the range of C_1-C_9), namely bio-oil, was analyzed through an offline GC-FID/MS instrument (Agilent 6890, 5973 MSD) equipped with an HP-5MS capillary column (30 m x 250 μm x 0.25 μm). This dual-detection setup enabled comprehensive analysis, with GC–MS providing qualitative identification of compounds based on a National Institute of Standards and Technology (NIST) mass spectral library, and GC-FID allowing for quantitative measurements after a dedicated calibration. Two distinct sampling protocols were then developed to collect, respectively, light and heavy condensable pyrolysis products for offline GC analysis. In particular, pyrolysis vapors were directly sampled from the outlet of the TGA when the devolatilization rate was maximum and were immediately injected into the GC using a gas syringe with a 2.5 ml volume. On the other hand, heavy products were collected using two Orbo-609 traps (Supelco) in series, containing Amberlite® XAD®-2 (400/200 mg), placed at the TGA outlet. After the experiments, the retained products were eluted from the sorbent material with a solution containing acetone and a known amount of 1-Fluoronaphthalene, used as an internal standard for the quantitative analysis in GC-FID. The obtained liquid mixture was then injected into the GC. Further details about the experimental setup can be found in [27].

Finally, a quadrupole mass spectrometer (HPR-20 EGA, Hiden Analytical) with a Secondary Electron Multiplier (SEM) detector was used for the monitoring of gaseous products (CO, CO_2, CH_4) and H_2O. This instrument was directly connected to the TGA chamber with a quartz inert capillary line, enabling real-time analysis of those products and direct association of their production dynamics with TG curves. The integral mass yield of these gaseous species was calculated after a proper calibration.

2.3. Lumped kinetic mechanism

The CRECK-S model offers a semi-detailed, multi-step approach, characterized by a lumped representation of products, thus providing a balance between accuracy and computational complexity. The CRECK-S model was initially developed using data from literature and has undergone continuous refinement over time [22–24]. Recent advancements in analytical equipment, such as thermogravimetric analysis coupled with product speciation techniques, have significantly enhanced the accuracy of pyrolysis experiments. This enables the detection and quantification of new species. For instance, a refined model for cellulose pyrolysis was recently proposed [28], incorporating new experimental evidence reported by Piazza et al. [27].

To better describe the atomic mass balances, the structural

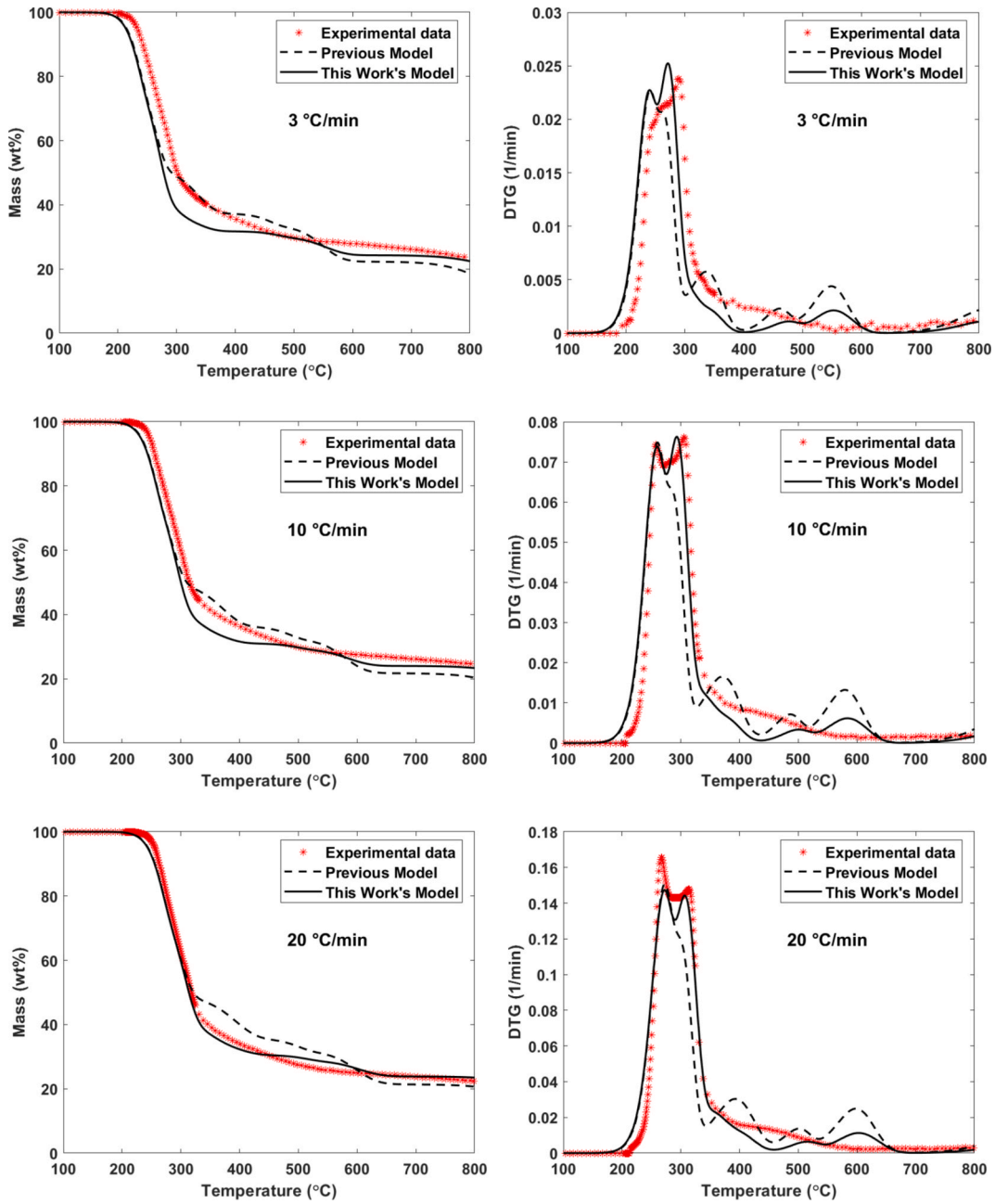

Fig. 3. Comparison of model prediction for TG (left) and DTG (right) curves for glucuronoxylan (GLXY) pyrolysis at 3, 10, 20, 50, 100 °C/min with experimental data and previous kinetic model [30].

composition of glucuronoxylan used in this work was refined. This component is heavily oxygenated with side groups of acetyl and glucuronic acid [29]. Therefore, a new reference species reflecting the elemental analysis shown in Table 1 was defined (GLXY, $C_5H_{10}O_5$).

The previous models particularly underestimate the yield of pyrolytic water and carbon monoxide (CO), while strongly overestimate tar yields (bio-oil). Char yields at pyrolysis temperatures above 750 °C are significantly underpredicted. To address these limitations and better capture the distribution of pyrolysis products, several improvements were implemented in this new kinetic model for glucuronoxylan as discussed in the following sentences. The overall structure of the multistep mechanism for hemicellulose was maintained. Additional volatile species were introduced into the model to account for the ketones and *cyclo*-oxygenates detected in the bio-oil fraction. The model was moreover modified to significantly reduce the yield of furans, acids and sugars, which are overpredicted by the previous mechanism.

Fig. 2a schematically shows the new CRECK-S model for glucuronoxylan pyrolysis. The reference species GLXY ($C_5H_{10}O_5$), representing glucuronoxylan, initially decomposes into two active intermediates: GLX1 and GLX2. These intermediates then undergo further decomposition through R2, R3 and R4, forming solid char and a range of condensable and non-condensable products. Fig. 2b shows the temperature dependency of the glucuronoxylan pyrolysis reactions, R1 to R4. GLX1 decomposes via two competing pathways, yielding most of the non-condensable gases from GLXY pyrolysis. Reaction R2, favored at temperatures above 300 °C, releases anhydrosugars and furans together with other light oxygenates and gases directly to the gas phase, without formation of metaplasts (e.g. G{species}). The competing reaction R3,

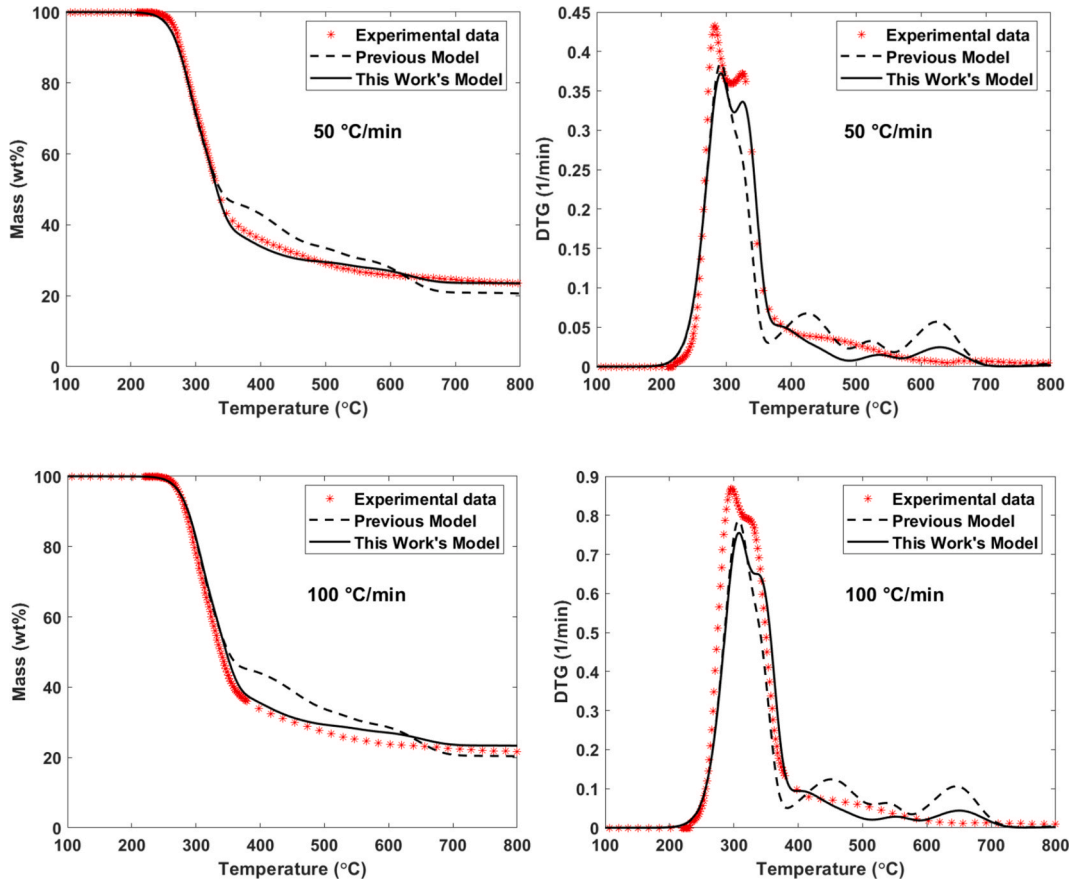

Fig. 3. (*continued*).

dominant below 300 °C (Fig. 2b), primarily produces light gaseous compounds and large amounts of metaplasts. These differences in selectivity aid the description of different product distribution in diverse pyrolysis regimes. GLX2, in contrast, produces most of the light oxygenated compounds such as ethanol (C_2H_5OH), glycolaldehyde (CH_2OHCHO), acetic acid (CH_3COOH), methyl-ethyl-ketone (MEK), together with pivalic acid ($C_5H_{10}O_2$), cyclopentanol (NC_5H_{10}-O), and char-trapped metaplasts that are released at high temperatures.

Table 2 presents the complete kinetic scheme for glucuronoxylan pyrolysis, formulated to describe its decomposition pathways and reaction kinetics. The mechanism accounts for the specific reactivities and decomposition profile of the glucuronoxylan chain, ensuring alignment with experimental observations.

Particularly, reaction R1 defines the initial breakdown of GLXY, with stoichiometry and kinetic parameters consistent with fundamental glucuronoxylan decomposition pathways. In reaction R2, the formation of anhydrosugars is limited, with $C_5H_8O_4$ representing their contribution. This minimal formation of anhydrosugars is balanced by increased formation of CO, H_2O, CH_3CHO, and CH_3COOH, reflecting their formation from alternative decomposition pathways. Additionally, furans formation is restricted to contributions from furfural ($C_5H_4O_2$). GLX1 decomposition via R2 also leads to the formation of CH_3COCH_3 (acetone), CO, H_2O, and char, better aligning the product slate with experimental data. Reaction R3 occurring at lower temperature conditions favors the formation of CO and CO_2 with a mild metaplastic species formation from GLX1. This leads to an increased release of H_2O and subsequent char formation. Reaction R4 involves the additional formation of small amounts of metaplastic species and strongly promotes the formation of H_2O, carbon monoxide (CO) and permanent char. It also accounts for the formation of other C_5 tar species (pivalic acid and *cyclo*-pentanol) as experimentally observed by Piazza et al. [18]. The formation of MEK (methyl-ethyl-ketone) is included to additionally reflect the contribution of ketones to the overall product mixture. The frequency factor for R4 is set as 5×10^9 [1/s] to improve the model's fit of the experimental DTG curve, specifically to better capture the dual-step decomposition behavior of glucuronoxylan pyrolysis.

Experimental findings indicate a delayed release of H_2O beyond the main decomposition peak (above 350 °C). To describe this feature, an additional metaplastic specie G{H_2O} is included in the model. Reaction R16 represents char dehydration and release of H2O at the beginning of the charring step (~400 °C).

3. Results and discussion

3.1. Comparison of experimental data and model predictions

3.1.1. TG and DTG curves

The performance of the new model in the prediction of mass loss was assessed. Fig. 3 shows a detailed one-to-one comparison between measured and calculated TG and DTG curves, where the response from the previous hemicellulose model [30] is also reported. The new model demonstrates an improved agreement with experimental data. The refined kinetic scheme accurately captures the primary mass loss phase between 200 °C and 350 °C. The onset and peak decomposition temperatures closely match experimental observations. Unlike the previous version, the new model corrects the overprediction of mass loss at high temperatures. This leads to char fractions that align more closely with experimental measurements and minimize deviations in the final mass loss.

The new model also more accurately captures the dual-stage decomposition behavior of glucuronoxylan as evident in the DTG curves, and minimizes the volatile release at high temperatures that

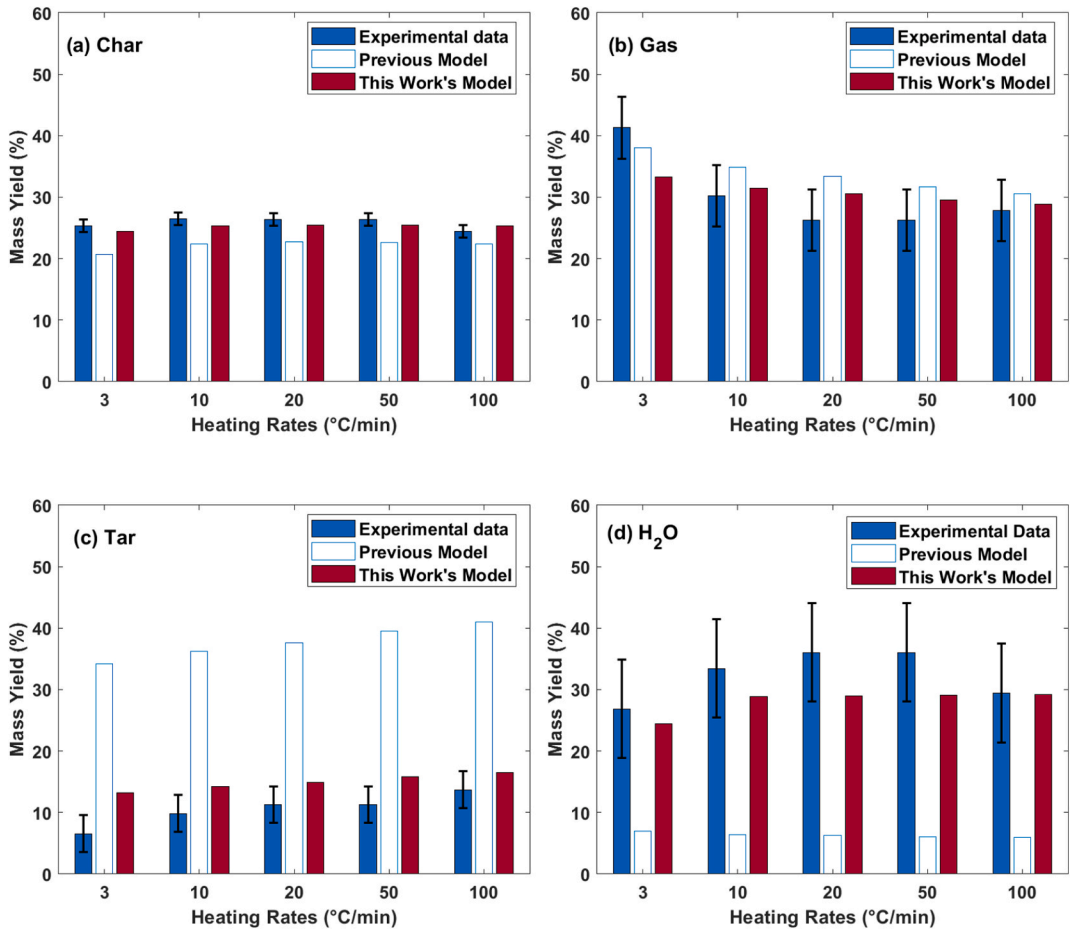

Fig. 4. Predicted integral mass yields of the main product categories of glucuronoxylan pyrolysis at 3, 10, 20, 50, 100 °C/min with experimental data and previous kinetic model [30].

previously led to overestimated mass loss. A similar behavior was observed for predictions at different heating rates.

3.1.2. Product speciation

Fig. 4 shows the new model predictions of the mass yields of major products compared to experimental data and the previous kinetic model. The new model demonstrates improved agreement across all product categories. Most importantly, as highlighted earlier, the previous model's poor prediction of liquid organic products and water yields was improved to match the experimental yields obtained. Additionally, the final char yield across the different heating rates more closely matches the experimental results than the previous model's prediction.

Fig. 5a compares then the predicted bio-oil product distribution from the new and previous models with the experimental data. The new model demonstrates significantly improved accuracy, aligning more closely with experimental observations. The predicted yields of furans, acids, and sugars have been reduced to better match the experimentally measured values. Additionally, the new model accounts for the formation of cyclic oxygenated compounds, exemplified by cyclopentanol, which were not present in the previous model. Fig. 5b compares the predictions of the new model with the previous model and experimental data, grouping the bio-oil species based on the length of their carbon chain. The overprediction of the previous model for C_1-C_3, C_5 and C_6, and the underrepresentation of C_4 was greatly improved in the new model. The predicted formation of C_6 species in the previous model was due to the interconnection between the scheme of the C_6-hemicellulose, GMSW (softwood hemicellulose) previously modelled as $C_5H_8O_4$ and that of XYHW (hardwood hemicellulose). The new model limits the prediction to C_5 species reflecting its exclusive focus on pentose hemicellulose. The formation of aromatics was also observed experimentally but is considered attributable to possible lignin residue in the xylan sample and, therefore, excluded in the new kinetic scheme.

Improvements are also evident in the prediction of gaseous products as shown in Fig. 5c. The new model more accurately estimates CO yields, bringing them in line with experimental values. Furthermore, the predicted yields of CO_2 and CH_4 have been slightly reduced compared to the prediction of the previous model. This resulted in a more balanced representation of the overall pyrolysis gas composition.

The ability of the model to capture the online release rates of key gaseous products and H_2O at different heating rates was also stringently verified, as shown in Fig. 6 (20 °C/min) and Fig. S1 (3 °C/min, 10 °C/min, 20 °C/min, 50 °C/min and 100 °C/min) in supplementary material. Both models capture the peak release temperature of the experimental measurements for all the heating rates. Compared to the previous model, the new model more accurately aligns with the release behavior of the experimental water measurements during both the main decomposition and initial charring steps. The new model limits the overprediction event of CO_2 between 380 °C to 520 °C and improves the peak release rate to match with the experimental release profile during the major devolatilization step. Additionally, improved prediction accuracy of CO yield is also obtained compared to the previous model. CH_4 is released in relatively small amounts across all heating rates. The new model predicts the release rate for CH_4 during the main decomposition step and at higher temperatures to be lower than the previous model's prediction, aligning closely with the experimental observations. Comparison with the experimental data suggests that CH_4 release is mostly related to char decomposition and likely occurs at lower temperatures than those predicted by the model. However, due to the limited yields of CH_4 (<2 wt%

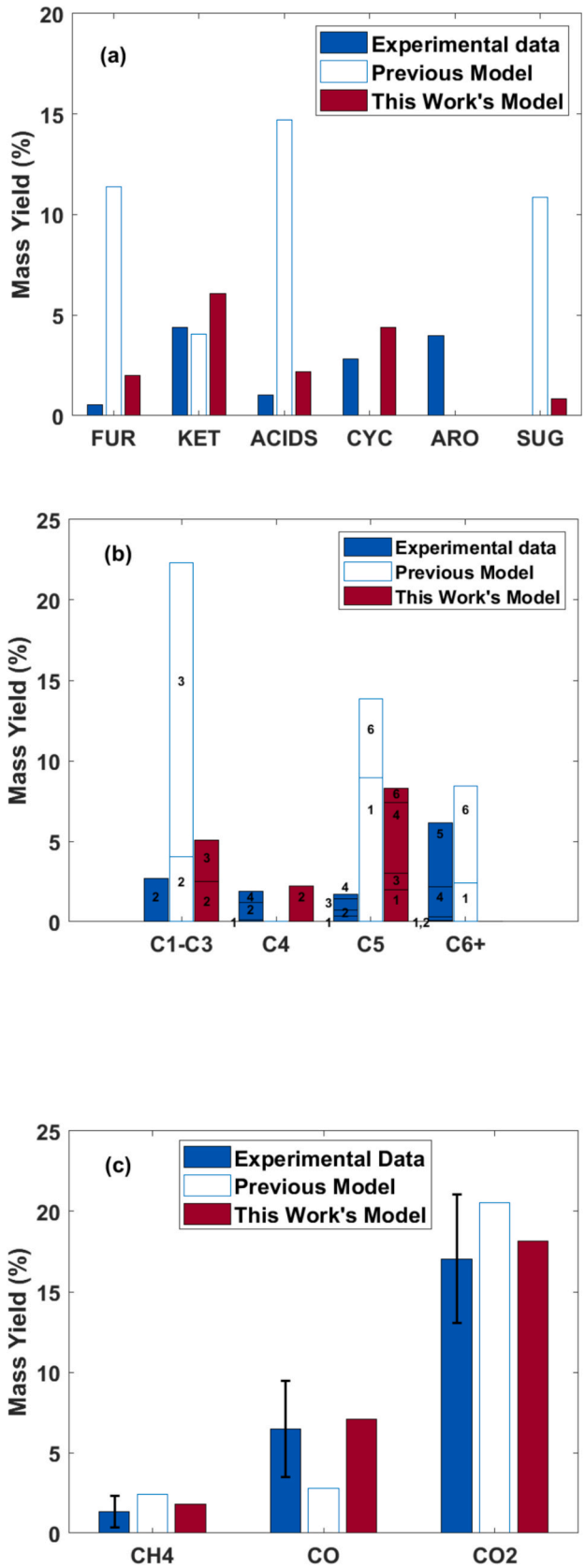

Fig. 5. (a)Speciation of glucuronoxylan bio-oil, (b) Yields of bio-oil fractions with different C-atoms [(1) Furans, (2) Aldehydes/ketones, (3) Acids/Alcohols, (4) Cyclo-oxygenates, (5) Aromatics, (6) Anhydrosugars], and (c) Yield of gaseous products. Both experiments and model simulations were obtained at at 100 °C/min.

of raw sample), we avoided further modifications in the reaction kinetics, so that the common release of the metaplastic species for other biomass reference species is maintained.

Table 3 shows the comparison of the elemental composition of the char obtained after pyrolysis up to 950 °C. The new model predicted the final C content to be 86.33 wt% which closely corresponds to the experimental value, and 9.96 wt% for O, slightly lower than the experimental value. The predicted content of H by the new model is 3.72 wt%, which is higher than the experimentally observed value of 0.35 %. Accelerating the decomposition of G{COH_2} species to temperatures below 800 °C could easily meet the measured values, but would lead to elevated H_2 gas yields, which contradict the same experiments. Nevertheless, typical amounts of H found in hemicellulose char samples range between 1.5–2 % [31] and in biomass char samples between 2–4 % [26], so we believe the low H content in char from the experiments is the possible result of underestimation error and, therefore, we prefer to maintain the model predictions in the current ranges. Compared to the predictions of the previous model of (69.67 wt% C and 27.35 wt% O), the new model exhibits a remarkable improvement in prediction accuracy of the char elemental composition.

3.2. *Validation by comparison with independent literature data*

To assess the reliability and accuracy in prediction of the new model, validation data available from the literature are also compared for mass loss curves at different heating rates. The products distribution for slow and flash pyrolysis experiments are also compared to provide a thorough assessment of the model's ability to capture the complex thermal decomposition behavior of glucuronoxylan.

3.2.1. *TG curves*

Experimental TG curves for glucuronoxylan pyrolysis at heating rates of 10 °C/min, 20 °C/min and 30 °C/min [9,32–35] were utilized for model validation. Fig. 7 presents the results of this comparison. The new kinetic model exhibits good agreement with the literature data across the investigated heating rates. The model's prediction of the onset temperature for glucuronoxylan decomposition closely matches the experimental data, accurately capturing the thermal stability of the glucuronoxylan structure and the initial breaking of glycosidic linkages. The model correctly reflects the influence of the heating rate on the pyrolysis behavior, shifting to higher temperatures as the heating rate increases. The mass loss curves predicted by the model closely align with the experimental curves during the primary decomposition stage (approximately 200–350 °C). This demonstrates the model's ability to represent the complex interplay of reactions that lead to the formation of volatile products during glucuronoxylan pyrolysis. Unlike the previous model, the new model aligns with experimental datasets in the char formation phase. It also adequately predicts the final char yield observed at higher temperatures.

The new model's performance was further tested at extreme operating range for glucuronoxylan torrefaction experiments performed by Kou and Chen [36,37], which involved a 1-hour torrefaction period. Notably, these experiments were also incorporated into the development of the previous model [23,30]. As shown in Fig. 8(a-b), the new model describes the overall torrefaction-pyrolysis process, capturing the initial moisture evaporation, the torrefaction phase, and the subsequent pyrolysis stage. The new model closely aligns with the previous model at lower torrefaction temperatures, with a pronounced deviation observed at 250 °C and 260 °C. The closer agreement of the previous model with the experimental data at these temperatures is attributable to the fact that the previous model was, in part, developed using these same experimental data. This might also suggest that this data exhibits some sort of behavior, such as large formations of metaplastic species during torrefaction that are subsequently rapidly released during pyrolysis, and are less obvious using the new model. This difference may stem from variations in the inherent characteristics of the xylan samples used in

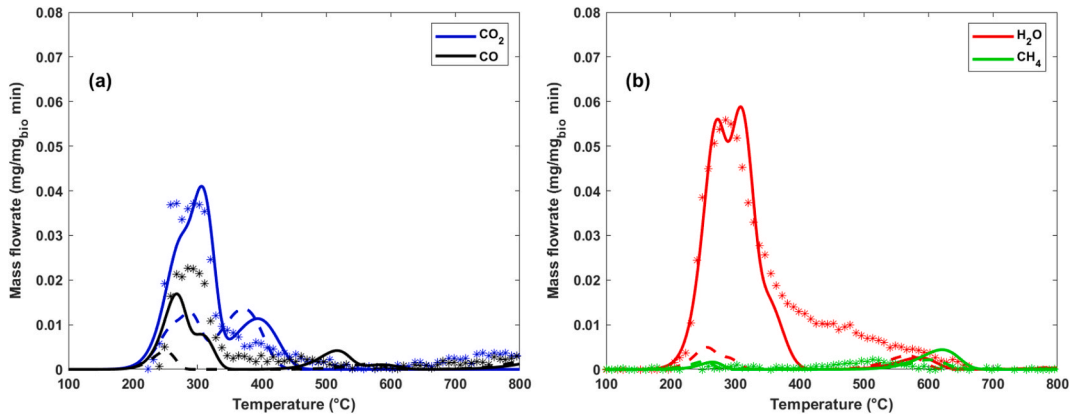

Fig. 6. Release rate of gaseous species (a) CO_2 and CO (b) H_2O and CH_4 for glucuronoxylan pyrolysis at 20 °C/min [symbols = experimental data, dashed lines = previous model [30] solid lines = this work's model].

Table 3
Elemental composition of char from pyrolysis at 100 °C/min up to 950 °C.

	C [wt%]	H [wt%]	N [wt%]	O [wt%]
Experiment	82.9	0.35	<0.1	16.75
Previous Model	69.67	2.98	0.0	27.35
This Work's model	86.33	3.72	0.0	9.96

this study compared to those employed by Kou and Chen [36,37], leading to differing thermal degradation characteristics.

3.2.2. Product distribution

The new kinetic model was further validated by comparing its predictions for the yields of H_2O, char, gases, and bio-oil, reported in the literature under a range of experimental conditions. Literature data on glucuronoxylan pyrolysis with detailed and quantitative product speciation are often scarce and the few available were used for the validation of this new model. These data, obtained from experiments in TGA set ups, fixed bed reactors, quartz tube reactors, and wire-mesh reactors across a temperature range of 500 °C to 700 °C as shown in Table S1 [18,38,39], provide an assessment of the model's performances across different reactor configurations and operating conditions. This comparison represents an extension of the 0-dimensional approach, initially applied to the TG experiments. In Fig. 9a, the yields of major products from the fixed bed experiment at 500 °C for 8.5 min by Piazza et al.[18] are in good agreement with the model predicted yields. Although the model predicts slightly higher yields of char and H_2O, and lower yields of gas and tar, compared to experimental values, these discrepancies are within the acceptable error tolerance of the lumped model approach. Additionally, potential errors introduced by simplifications in the reactor model, such as heat and mass transfer limitations, may also contribute to these minor deviations. The corresponding predicted yields of the bio-oil and gaseous fractions (Fig. 9b) from the same experiment shows that the model can well predict the yields of the various fractions in fixed bed reactors, showing a clear improvement with respect to the previous version of the model.

The results from another fixed bed experiment in Fig. 10(a-b) by Stefanidis et al.[38] demonstrate the ability of the model to predict the yields with a reasonable accuracy, in the absence of quantified experimental uncertainties· H_2O and gas predictions align well with the experimental observations. The predictions for char and tar show the model's response represents the balance between this experiment and that of Piazza et al. [18]. The model accurately predicted the yield of furans and ketones/aldehydes as shown in Fig. 9b.

3.2.3. Product distribution at high heating rates

Char formation from glucuronoxylan fast pyrolysis was assessed by comparison with measurements from Shen et al. [7] across different conditions of temperature in quartz tube flow reactor within a short residence time of 0.5 s (allowing for 30 s cooling time in the simulation). While the simulation assumes negligible reactor model effects, which may introduce some inaccuracies, the model approximately captures the char yields observed experimentally from 510 °C to 690 °C as shown in Fig. 11.

To conclude, comparison of yield of products from fast pyrolysis was assessed with measurements from Hoekstra et al. [40] in a wire mesh reactor at high heating rates of 6000 °C/s and 1 s holding time. The results of the simulation at these conditions (allowing 60 s for cooling to room temperature) are plotted in Fig. 12. A good agreement between the two results can be observed for the main pyrolysis products and the distribution of gaseous products (CO and CO_2), also considering possible experimental uncertainty.

Statistical comparison using Pearson correlation-based dissimilarity indices and sum-of-squared-error metrics are used to evaluate the overall performance of the new kinetic model relative to the previous model. The overall TGA curve matching index parameter M across the investigated heating rates as shown in Fig. S2(a) and the dissimilarity indices shown in Table S2 demonstrated the superior prediction capability of the new model (with M ranging from 0.776 to 0.885) against the previous model (with M ranging from 0.714 to 743). Additional comparison of the model performance is shown in Fig. S2(b–d) where the new model's sum of squared errors for product distributions from this work (Figs. 4-5) and from other works (Figs. 9-12) were significantly lower than the previous model's, confirming its improved accuracy in predicting yields and represents a major advancement in simulating xylan pyrolysis across various conditions and reactor set-ups.

3.3. Mechanistic considerations for glucuronoxylan pyrolysis

To better elucidate the improvements introduced by the refined model, a brief discussion on the underlying reaction mechanisms is here presented.

The first reaction proposed in the model (R1) represents the activation of glucuronoxylan. This is the step with the highest activation energy and begins at temperatures below 200 °C, as shown in Fig. 13.

Below 250 °C, dehydration reactions and the cleavage of weaker bonds associated with lateral substituents begin to occur. These processes are represented in the model by reactions R3 and, to some extent, R2. Dehydration reactions play a dominant role [7,41], contributing significantly to the release of H_2O captured in R3. Compared to previous models, the extent of water release has been notably increased to more accurately reflect the experimental data. The fragmentation of the

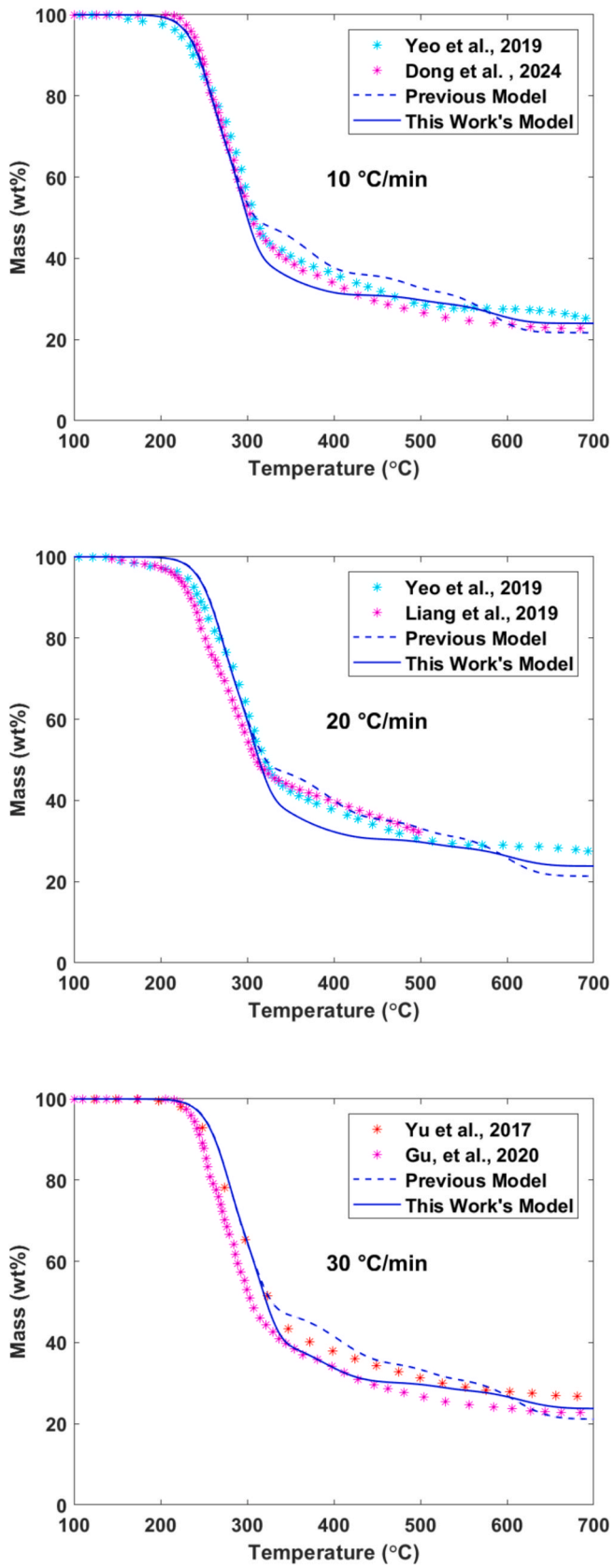

Fig. 7. TG curves at different heating rates [9,32–35].

methoxy group attached to the C4 position of the glucuronic acid unit results in the formation of methanol (R2) [7,41]. Instead, the decomposition of acetyl groups, accounting for approximately 11.4 wt% of total xylan, leads to the generation of acetic acid (R2) [41]. Moreover, the decarboxylation of the carboxylic acid moiety contributes to the early formation of CO and CO_2, with their release primarily associated with reaction R3 [7,41].

Between 250 °C and 350 °C, the glycosidic linkages in the xylan backbone become increasingly unstable, initiating the depolymerization processes [7,21,41], represented in the model by reactions R2 and R4. Depolymerization leads to the formation of 1,4-anhydro-β-D-xylopyranose [21]. However, this compound is relatively unstable and is rarely detected in pyrolysis oils. Instead, it rapidly decomposes into smaller oxygenated species and gases, acting as a transient intermediate [21]. A sugar-like compound ($C_5H_8O_4$), is still included in reaction R2 to account for its presence. Compared to previous models, however, its yield has been significantly reduced, in favor of increased formation of CO, H_2O, acetaldehyde (CH_3CHO), and acetic acid (CH_3COOH), consistent with experimental observations.

The primary C_5 products resulting from xylan depolymerization are furanic compounds, derivatives of the pentose sugars that constitute the xylan backbone [7,21,41]. These species are formed through ring-opening and rearrangement reactions of xylan monomers and are represented in the proposed mechanism by FURFURAL, produced via reaction R2.

In addition to furans, other condensable products commonly observed include aldehydes, ketones, and acetic compounds [7,21,41]. To better align with experimental data, the current mechanism introduces in R4 a cyclic oxygenate (cyclopentanol) and two ketones, methyl ethyl ketone and butanedione.

Finally, the rapid depolymerization of the xylan structure also generates a significant amounts of H_2O, CO_2, and CO, and these are accounted for in both R2 and R4.

At temperatures exceeding 350 °C, reactions R5-R16 generate gaseous species. These originate from the release of metaplastic species, intermediates that were retained within the solid matrix at lower temperatures during the rearrangement of the solid phase (as described by reactions R3 and R4).

Finally, glucuronoxylan produces a substantial amount of char, a behavior commonly associated with the amorphous nature of hemicellulosic polymers [41]. To reflect this behavior, char production is included in all reactions stemming from the intermediates GLX1 and GLX2 (reactions R2–R4). Compared to previous models, the char yield has been increased in accordance with experimental observations.

4. Conclusions

This work presents a new kinetic model for the pyrolysis of glucuronoxylan, a key component of hardwood hemicellulose, leveraging a novel TGA-based experimental methodology. The model, developed using high-precision experimental data, significantly improves the prediction of devolatilization rates, product yields, and speciation compared to previous models.

Relying on newly collected data on devolatilization rates, the refined kinetic model is able to effectively capture the dual-stage decomposition behavior of glucuronoxylan, accurately predicting the onset and peak decomposition temperatures across different heating rates (3 °C/min to 100 °C/min). In addition, a comprehensive and quantitative experimental analysis on product distribution has further improved model predictions of key pyrolysis products. For instance the final char and water yields have been significantly increased, and gas products distribution has been improved. Bio-oil yield has been decreased, and some new components have been included to reflect experimental evidence. Moreover, the model's ability to predict the release rates of gaseous species (CO, CO_2, CH_4, and H_2O) and their temperature-dependent evolution further underscores its reliability.

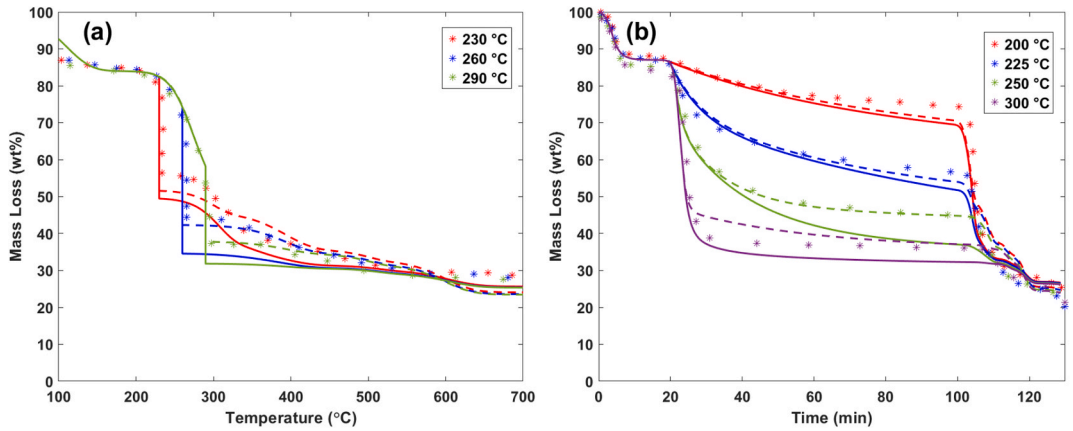

Fig. 8. Comparison of model performance for xylan at different torrefaction temperatures [36,37] [Scatter = experimental data, dashed lines = previous model and solid lines = This work's model].

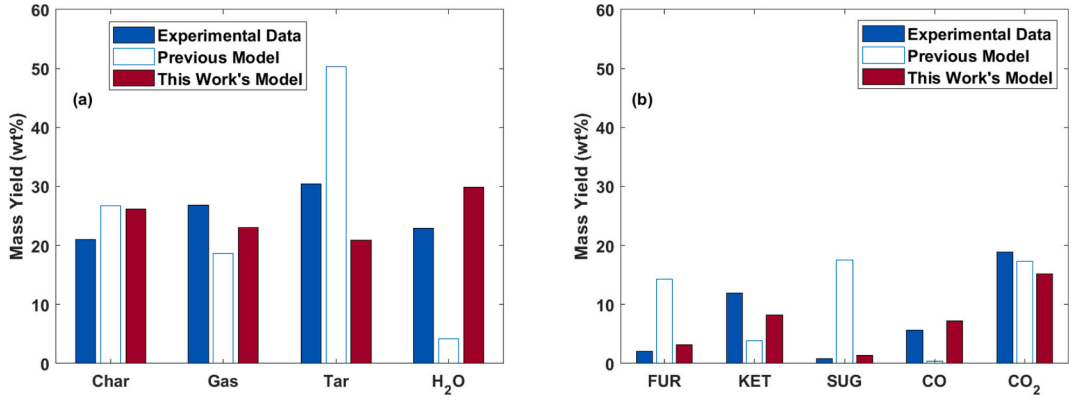

Fig. 9. Product distribution from glucuronoxylan pyrolysis in fixed bed reactor [500 °C, 8.5 min] by Piazza et al.[18]: (a) Yield of main pyrolysis products (b) Yield of Bio-oil and Gaseous Products.

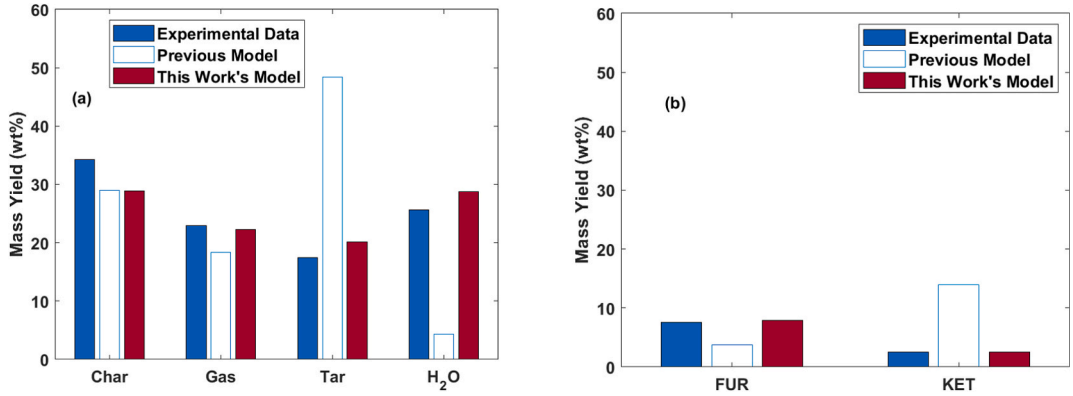

Fig. 10. Product distribution from glucuronoxylan pyrolysis in fixed bed reactor [500 °C, 15 min] by Stefanidis et al. [38]: (a) yield of main pyrolysis products, (b) yield of bio-oil products.

Validation against literature data from diverse pyrolysis regimes including torrefaction (200 °C to 300 °C for 1 h), slow (10 °C/min to 30 °C/min), fast (isothermal at 500 °C) and flash pyrolysis (>10^3 °C/s) regimes using various reactor configurations (including TGA, fixed bed, quartz tube, and wire-mesh reactors), confirms the model's versatility and accuracy in predicting product distributions under different experimental conditions. The model's improved performance in predicting char elemental composition of 86.3 % C versus experimental value of 82.9 % at high temperatures further highlights its potential for optimizing biomass conversion processes. Statistical comparison confirms the new model's superior prediction accuracy, with a matching factor of 0.776–0.885 for TGA curve prediction against the previous model's range of 0.714–0.743, and a significantly lower SSE value for prediction of product distributions.

This study provides a comprehensive and reliable kinetic model for glucuronoxylan pyrolysis, offering valuable insights into the thermal decomposition of hemicellulose. The model serves as a robust tool for the design and optimization of thermochemical conversion processes,

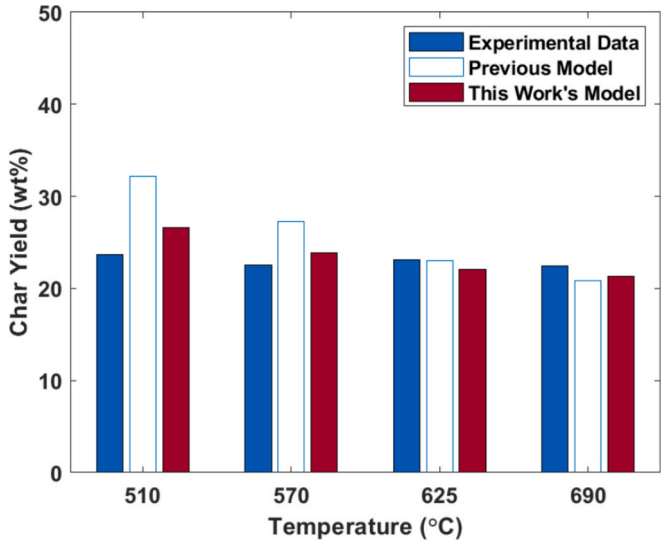

Fig. 11. Yield of Char from glucuronoxylan pyrolysis in quartz tube reactor, 0.5 s from Shen et al.[7].

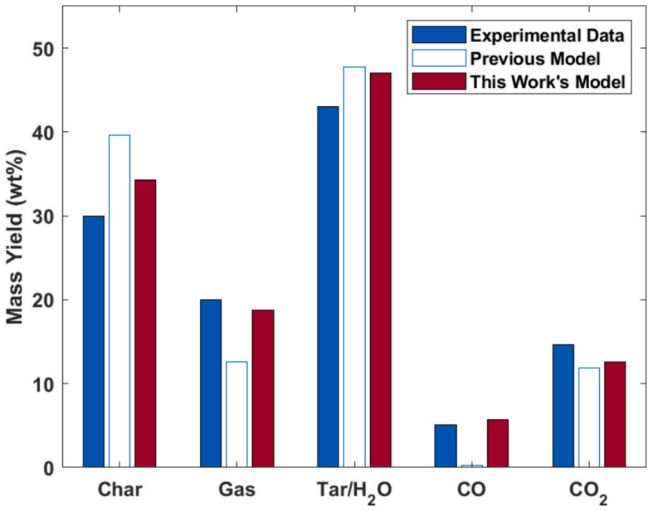

Fig. 12. Product Distribution from wire mesh reactor: 6000 °C/s, 1 s holding time [40].

contributing to the advancement of bioenergy and bio-based chemical production. Future work will focus on extending this modeling approach to other hemicellulose types and integrating it into broader biomass pyrolysis frameworks to further enhance the predictive capabilities for complex biomass feedstocks.

CRediT authorship contribution statement

Muhammad Yusuf Suleiman: Writing – original draft, Validation, Investigation, Formal analysis, Data curation, Conceptualization. **Eleonora Benedetto:** Writing – original draft, Validation, Investigation, Formal analysis, Data curation, Conceptualization. **Veronica Piazza:** Writing – review & editing, Writing – original draft, Visualization, Validation, Supervision, Investigation, Formal analysis, Data curation, Conceptualization. **Luca Lietti:** Resources, Project administration, Funding acquisition, Writing – review & editing, Visualization, Supervision. **Alessio Frassoldati:** Writing – review & editing, Visualization, Supervision, Resources, Project administration, Funding acquisition. **Tiziano Faravelli:** Writing – review & editing, Visualization, Supervision, Project administration, Methodology, Funding acquisition, Conceptualization. **Alessandra Beretta:** Writing – review & editing, Visualization, Supervision, Project administration, Methodology, Conceptualization. **Paulo Debiagi:** Visualization, Project administration, Investigation, Validation, Methodology, Funding acquisition, Writing – review & editing, Writing – original draft, Conceptualization.

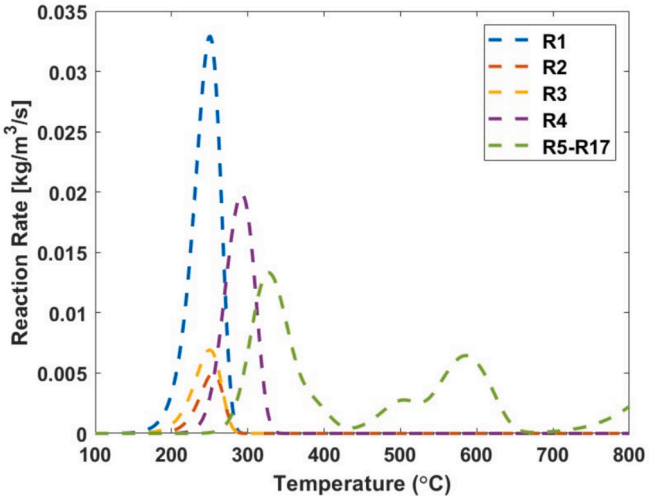

Fig. 13. Temperature dependence of proposed reaction rates.

Declaration of competing interest

The authors declare that they have no known competing financial interests or personal relationships that could have appeared to influence the work reported in this paper.

Acknowledgments

This study was partially conducted within the Agritech National Research Center and received funding from the European Union (1) Next-GenerationEU (PNRR) – MISSIONE 4 COMPONENTE 2, INVESTIMENTO 1.4 and 1.3 – D.D. 1032 17/06/2022, CN00000022, and (2) Pysolo project (Grant Agreement n. 101118270). Views and opinions expressed are however those of the author(s) only and do not necessarily reflect those of the European Union or CINEA. Neither the European Union nor the granting authority can be held responsible for them.

Appendix A. Supplementary data

Supplementary data to this article can be found online at https://doi.org/10.1016/j.ecmx.2025.101130.

Data availability

Data will be made available on request.

References

[1] World Energy. Outlook 2022;www.iea.org/t&c/.
[2] M. R. Chandraratne, A. G. Daful, Recent Advances in Thermochemical Conversion of Biomass, in: Recent Perspectives in Pyrolysis Research, IntechOpen, 2022. https://doi.org/10.5772/intechopen.100060.
[3] Sherwood J. The significance of biomass in a circular economy. Bioresour. Technol. 2020;300. https://doi.org/10.1016/j.biortech.2020.122755.
[4] Khater E-S, Bahnasawy A, Hamouda R, Sabahy A, Abbas W, Morsy OM. Biochar production under different pyrolysis temperatures with different types of agricultural wastes. Sci. Rep. 2024;14:2625. https://doi.org/10.1038/s41598-024-52336-5.
[5] Srivastava N, Shrivastav A, Singh R, Abohashrh M, Srivastava KR, Irfan S, et al. Advances in the Structural Composition of Biomass. Fundamental and Bioenergy Applications, J Renew Mater 9 2021:615–36. https://doi.org/10.32604/jrm.2021.014374.

[6] Rao J, Lv Z, Chen G, Peng F. Hemicellulose: Structure, chemical modification, and application. Prog. Polym. Sci. 2023;140. https://doi.org/10.1016/j.progpolymsci.2023.101675.
[7] Shen DK, Gu S, Bridgwater AV. Study on the pyrolytic behaviour of xylan-based hemicellulose using TG-FTIR and Py-GC-FTIR. J. Anal. Appl. Pyrolysis 2010;87:199–206. https://doi.org/10.1016/j.jaap.2009.12.001.
[8] Smith MW, Pecha B, Helms G, Scudiero L, Garcia-Perez M. Chemical and morphological evaluation of chars produced from primary biomass constituents: Cellulose, xylan, and lignin. Biomass Bioenergy 2017;104:17–35. https://doi.org/10.1016/j.biombioe.2017.05.015.
[9] Yu J, Paterson N, Blamey J, Millan M. Cellulose, xylan and lignin interactions during pyrolysis of lignocellulosic biomass. Fuel 2017;191:140–9. https://doi.org/10.1016/j.fuel.2016.11.057.
[10] Usino DO, Supriyanto P, Ylitervo A, Pettersson TR. Influence of temperature and time on initial pyrolysis of cellulose and xylan. J Anal Appl Pyrolysis 147 2020. https://doi.org/10.1016/j.jaap.2020.104782.
[11] Wang S, Ru B, Lin H, Luo Z. Degradation mechanism of monosaccharides and xylan under pyrolytic conditions with theoretic modeling on the energy profiles. Bioresour. Technol. 2013;143:378–83. https://doi.org/10.1016/j.biortech.2013.06.026.
[12] Ye ZH, Zhong R. Outstanding questions on xylan biosynthesis. Plant Sci. 2022;325. https://doi.org/10.1016/j.plantsci.2022.111476.
[13] Mortimer JC, Faria-Blanc N, Yu X, Tryfona T, Sorieul M, Ng YZ, et al. An unusual xylan in Arabidopsis primary cell walls is synthesised by GUX3, IRX9L, IRX10L and IRX14. Plant J. 2015;83:413–26. https://doi.org/10.1111/tpj.12898.
[14] Ayarde-Henríquez L, Lupi J, Dooley S. Hemicellulose pyrolysis: mechanism and kinetics of functionalized xylopyranose. PCCP 2024;26:12820–37. https://doi.org/10.1039/D3CP06094B.
[15] Chen D, Cen K, Zhuang X, Gan Z, Zhou J, Zhang Y, et al. Insight into biomass pyrolysis mechanism based on cellulose, hemicellulose, and lignin: Evolution of volatiles and kinetics, elucidation of reaction pathways, and characterization of gas, biochar and bio-oil. Combust. Flame 2022;242. https://doi.org/10.1016/j.combustflame.2022.112142.
[16] Zhou X, Li W, Mabon R, Broadbelt LJ. A critical review on hemicellulose pyrolysis. Energ. Technol. 2017;5:52–79. https://doi.org/10.1002/ente.201600327.
[17] Rong Wang S, Liang T, Ru B, Juan Guo, X. echanism of xylan pyrolysis by Py-GC/MS. Chem. Res. Chin. Univ. 2013;29:782–7. https://doi.org/10.1007/s40242-013-2447-6.
[18] Piazza V, Batista da Silva Junior R, Frassoldati A, Lietti L, Gambaro C, Rajendran K, Chen D, Faravelli T, Beretta A. Unravelling the complexity of hemicellulose pyrolysis: Quantitative and detailed product speciation for xylan and glucomannan in TGA and fixed bed reactor. Chemical Engineering Journal 497 2024:154579. https://doi.org/10.1016/J.CEJ.2024.154579.
[19] Werner K, Pommer L, Broström M. Thermal decomposition of hemicelluloses. J. Anal. Appl. Pyrolysis 2014;110:130–7. https://doi.org/10.1016/j.jaap.2014.08.013.
[20] Duan J, Hu H, Ji J. Mechanism study on arabinose pyrolysis by combining TG-FTIR-GC–MS and theoretical calculations. Combust. Flame 2022;245. https://doi.org/10.1016/j.combustflame.2022.112352.
[21] Hu B, Lu Q, Zhang ZX, Wu YT, Li K, Dong CQ, et al. Mechanism insight into the fast pyrolysis of xylose, xylobiose and xylan by combined theoretical and experimental approaches. Combust. Flame 2019;206:177–88. https://doi.org/10.1016/j.combustflame.2019.04.052.
[22] T. Faravelli, A. Frassoldati, E. Barker Hemings, E. Ranzi, Multistep kinetic model of biomass pyrolysis, in: Green Energy and Technology, Springer Verlag, 2013: pp. 111–139. https://doi.org/10.1007/978-1-4471-5307-8_5.
[23] Debiagi P, Gentile G, Cuoci A, Frassoldati A, Ranzi E, Faravelli T. A predictive model of biochar formation and characterization. J. Anal. Appl. Pyrolysis 2018;134:326–35. https://doi.org/10.1016/j.jaap.2018.06.022.
[24] Ranzi E, Cuoci A, Faravelli T, Frassoldati A, Migliavacca G, Pierucci S, et al. Chemical kinetics of biomass pyrolysis. Energy Fuels 2008;22:4292–300. https://doi.org/10.1021/ef800551t.
[25] Ranzi E, Debiagi PEA, Frassoldati A. Mathematical Modeling of Fast Biomass Pyrolysis and Bio-Oil Formation. Note i: Kinetic Mechanism of Biomass Pyrolysis, ACS Sustain Chem Eng 2017;5:2867–81. https://doi.org/10.1021/acssuschemeng.6b03096.
[26] Dussan K, Dooley S, Monaghan R. Integrating compositional features in model compounds for a kinetic mechanism of hemicellulose pyrolysis. Chem. Eng. J. 2017;328:943–61. https://doi.org/10.1016/J.CEJ.2017.07.089.
[27] Piazza V, da Silva Junior RB, Frassoldati A, Lietti L, Chiaberge S, Gambaro C, et al. Detailed speciation of biomass pyrolysis products with a novel TGA-based methodology: the case-study of cellulose. J Anal Appl Pyrolysis 178 2024. https://doi.org/10.1016/j.jaap.2024.106413.
[28] Debiagi P, Piazza V, Papagni M, Beretta A, Frassoldati A, Faravelli T. Cellulose pyrolysis kinetic model: Detailed description of volatile species. Proc. Combust. Inst. 2024;40. https://doi.org/10.1016/j.proci.2024.105651.
[29] Wang S, Ru B, Lin H, Sun W. Pyrolysis behaviors of four O-acetyl-preserved hemicelluloses isolated from hardwoods and softwoods. Fuel 2015;150:243–51. https://doi.org/10.1016/j.fuel.2015.02.045.
[30] Afessa MM, Locaspi A, Debiagi P, Frassoldati A, Caraccio R, Ramayya AV, et al. Pyrolysis of large biomass particles: Model validation and application to coffee husks valorization. J. Anal. Appl. Pyrolysis 2025;188. https://doi.org/10.1016/j.jaap.2025.107028.
[31] Magalhães D, Gürel K, Matsakas L, Christakopoulos P, Pisano I, Leahy JJ, et al. Prediction of yields and composition of char from fast pyrolysis of commercial lignocellulosic materials, organosolv fractionated and torrefied olive stones. Fuel 2021;289. https://doi.org/10.1016/j.fuel.2020.119862.
[32] Dong Z, Wei Y, Chen Y, Zhang L, Xu D, Lin G, et al. Nitrogen migration and transformation in chars and tars during co-pyrolysis of cellulose/xylan/lignin with urea formaldehyde. J Anal Appl Pyrolysis 178 2024. https://doi.org/10.1016/j.jaap.2024.106425.
[33] Yeo JY, Chin BLF, Tan JK, Loh YS. Comparative studies on the pyrolysis of cellulose, hemicellulose, and lignin based on combined kinetics. J. Energy Inst. 2019;92:27–37. https://doi.org/10.1016/j.joei.2017.12.003.
[34] Liang J, Chen J, Wu S, Liu C, Lei M. Comprehensive insights into xylan structure evolution via multi-perspective analysis during slow pyrolysis process. Fuel Process. Technol. 2019;186:1–7. https://doi.org/10.1016/j.fuproc.2018.12.014.
[35] Gu J, Fan H, Wang Y, Zhang Y, Yuan H, Chen Y. Co-pyrolysis of xylan and high-density polyethylene: product distribution and synergistic effects. Fuel 2020;267. https://doi.org/10.1016/j.fuel.2019.116896.
[36] Chen WH, Kuo PC. Isothermal torrefaction kinetics of hemicellulose, cellulose, lignin and xylan using thermogravimetric analysis. Energy 2011;36:6451–60. https://doi.org/10.1016/j.energy.2011.09.022.
[37] Chen WH, Kuo PC. Torrefaction and co-torrefaction characterization of hemicellulose, cellulose and lignin as well as torrefaction of some basic constituents in biomass. Energy 2011;36:803–11. https://doi.org/10.1016/j.energy.2010.12.036.
[38] Stefanidis SD, Kalogiannis KG, Iliopoulou EF, Michailof CM, Pilavachi PA, Lappas AA. A study of lignocellulosic biomass pyrolysis via the pyrolysis of cellulose, hemicellulose and lignin. J. Anal. Appl. Pyrolysis 2014;105:143–50. https://doi.org/10.1016/j.jaap.2013.10.013.
[39] Gargiulo V, Ferreiro AI, Giudicianni P, Tomaselli S, Costa M, Ragucci R, et al. Insights about the effect of composition, branching and molecular weight on the slow pyrolysis of xylose-based polysaccharides. J. Anal. Appl. Pyrolysis 2022;161. https://doi.org/10.1016/j.jaap.2021.105369.
[40] Hoekstra E, Van Swaaij WPM, Kersten SRA, Hogendoorn KJA. Fast pyrolysis in a novel wire-mesh reactor: Decomposition of pine wood and model compounds. Chem. Eng. J. 2012;187:172–84. https://doi.org/10.1016/j.cej.2012.01.118.
[41] Collard FX, Blin J. A review on pyrolysis of biomass constituents: Mechanisms and composition of the products obtained from the conversion of cellulose, hemicelluloses and lignin. Renew. Sustain. Energy Rev. 2014;38:594–608. https://doi.org/10.1016/j.rser.2014.06.013.